Perpendicular magnetic anisotropy in CoFe/MgO/CoFe magnetic tunnel junctions by first-principles calculations

Jia Zhang,* Christian Franz, Michael Czerner, and Christian Heiliger†
I. Physikalisches Institut, Justus Liebig University Giessen, Heinrich-Buff-Ring 16, 35392 Giessen, Germany
(Received 28 August 2014; revised manuscript received 22 October 2014; published 7 November 2014)

The magnetic anisotropy in Fe_xCo_{100-x}/MgO/Fe_xCo_{100-x} magnetic tunnel junctions as a function of composition is investigated on different substrates (Cu, Ag, and MgO). We use the full relativistic screened-Korringa-Kohn-Rostoker method and employ the coherent potential approximation for description of the alloys. Our findings show that the magnetocrystalline anisotropy (MCA) strongly depends on the CoFe composition and that the MCA decreases with increasing Co concentration. At a certain composition there is a transition at which the MCA changes sign from positive to negative. The origin of the MCA is related to the difference of density of states between d orbitals around Fermi energy, in particular, the difference between $d_{yz}(d_{zx})$ and $d_{3z^2-r^2}$ orbitals. We also calculate the shape anisotropy in order to obtain phase diagrams that show at which magnetic layer thickness and at which composition we expect perpendicular anisotropy.

DOI: 10.1103/PhysRevB.90.184409 PACS number(s): 75.30.Gw, 72.25.−b, 73.40.Rw, 75.70.Cn

Magnetic tunnel junctions (MTJs) with perpendicular magnetic anisotropy (PMA) are considered to be good candidates to meet the needs for ultrahigh density storage and low current switching devices [1–3]. Recently, it was demonstrated experimentally that PMA and low current switching can be realized in MgO-MTJs by using ultrathin CoFeB magnetic layers as electrodes [3,4]. Different from traditional PMA-MTJs that use CoPt, FePt, etc. as electrodes [5–7], CoFeB/MgO/CoFeB is an ideal MTJ structure, because of its high tunneling magneto-resistance (TMR) [8] and the absence of noble metals.

Great efforts have been made since the discovery of large PMA effects in CoFeB/MgO. Many experimental factors were found to have strong influence on PMA including annealing temperature [9], capping layer [10], substrates [11], and interface insertion layer [12], as well as CoFeB composition [4]. The magnetic anisotropic energy (MAE) in CoFeB-MgO system is estimated to be as large as 1–2 erg/cm^2. The PMA in magnetic multilayers is a consequence of the competition between the magnetocrystalline anisotropy energy (MCA) and shape anisotropy energy (or demagnetization energy). The MCA can be calculated explicitly by using first-principles calculations [13–15]. Recently, Yang *et al.* carried out first-principles calculations to investigate the origin of perpendicular MAE in Fe/MgO/Fe-MTJs [16]. The role of the Fe-MgO interface bonding was emphasized and the MAE was attributed to the overlap between the p_z orbital of O in the MgO interface layer and the $d_{3z^2-r^2}$ orbital in Fe.

The alloy composition of magnetic electrodes in MTJs is crucial for spin dependent transport. It was shown both from theory [17,18] and experiment [8,19,20] that the spin dependent transport in CoFeB or CoFe/MgO/CoFe-MTJs are strongly dependent on the alloy composition. For instance, the highest TMR at room temperature have been achieved in CoFeB/MgO/CoFeB-MTJs with $Co_{20}Fe_{60}B_{20}$ as electrodes [8]. Recent experiments show also for the PMA a composition dependence [4,21]. In particular, a decrease of PMA with increasing Co concentration is reported [4,21]. However, there is no explanation. Consequently, first-principle calculations are necessary to explore the PMA effect in CoFe/MgO/CoFe-MTJs.

For the first-principles calculations of the anisotropy we use the full relativistic screened-Korringa-Kohn-Rostoker (KKR) method based on spin density functional theory (SDFT). The spin-orbit coupling is taken into account by solving the full relativistic Dirac equation [24].

The potentials are described within the atomic sphere approximation (ASA). For the calculations we use a symmetric supercell sketched in Fig. 1. The in-plane lattice constant of the whole junction is fixed to the bulk lattice constant of Fe (2.866 Å). We calculate the MCA by using the magnetic force theorem [13–15]. This method has been successfully adopted to calculate the MCA of ferromagnetic multilayer films. First, the self-consistent atomic potential is obtained by performing a scalar-relativistic calculation. Then one-step full relativistic calculation is performed along two different magnetic directions to obtain the band energy. Eventually, the MCA is determined by the band energy difference MAE = $E_{\text{band}}(\parallel) - E_{\text{band}}(\perp)$, where $\parallel$ and $\perp$ indicate if the magnetic moment of the magnetic layer is parallel or perpendicular to the film interface as it is shown in Fig. 1. Sixty energy points in the complex plane and 120×120 k points in the two-dimensional Brillouin zone have been chosen to get the MCA converged within 1 μeV per atom. We use the coherent potential approximation (CPA) to describe the composition dependence of the FeCo alloys on the MCA. The KKR-CPA method is used for calculating the MCA for different magnetic multilayered structures [13–15]. The demagnetization energy (or shape anisotropy) is calculated by summing the magnetic dipole interaction on each layer [13]. Finally, we obtain the critical thickness with PMA by summing MCA and shape anisotropy energy.

The FeCo composition dependence of the MCA for different substrates (Cu, Au, and MgO) are shown in Fig. 2. First we can see for the MTJs on Cu and MgO substrates, i.e., no noble metal atoms, the MCA is quite large and they are even larger than the MCA in typical FM/noble metal system,

*jia.zhang@exp1.physik.uni-giessen.de
†christian.heiliger@physik.uni-giessen.de

 ©2014 American Physical Society

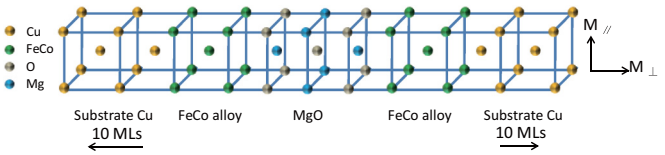

FIG. 1. (Color online) Illustration of atomic structure used for the present calculation.

for instance Co/Pt(111) and Co/Pd(111), which have MCA value around 1 erg/cm^2 (see Table I for reference). Second, the MCA decreases with increasing Co content and there is a transition content where MCA change sign. For example, on Cu substrate, when the Fe content decreases from 70% to 10%, the MCA decreases drastically and has a transition from positive to negative values at $Fe_{40}Co_{60}$. The decrease of MCA at the CoFeB/MgO interface has been reported experimentally by Yakata *et al.* [4]. Similar behavior of the composition dependence of the MCA is found for CoFe monolayer and clusters on Cu(001) [25]. Interestingly, we find that with Au substrate the MCA of the junction is smaller than that with Cu substrate and the MCA decreases with increasing Co content with a slower slope. For Au substrate, the content of Fe should be larger than 70% to have positive MCA. In addition, the comparison between the present calculation and available experiment results are listed in Table I. One can see that our calculations are in very good quantitative agreement to experiment and can therefore be used to predict PMA in other magnetic layers.

The easy axis of a magnetic thin film is not only determined by MCA but also by the shape anisotropy energy (SAE). From the microscopic mechanism, the shape anisotropy energy originates from the Breit interaction and is not included in spin density based first-principles calculation [26]. In the present paper we calculate the SAE by summing the magnetostatic dipole-dipole interaction between atomic magnetic moments [13].

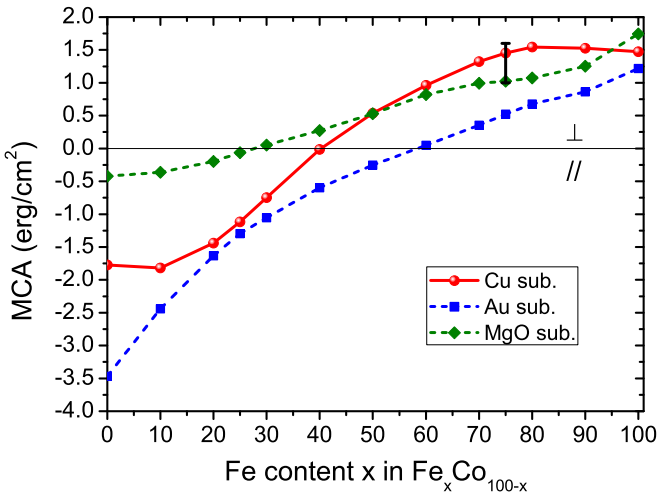

FIG. 2. (Color online) MCA per interface in (Cu,Au,MgO)/Fe_xCo_{100-x}(3 MLs)/MgO(3 MLs)/ Fe_xCo_{100-x}(3 MLs)/(Cu, Au, MgO) junctions as a function of Fe composition in CoFe. The vertical black line indicates the experimental MCA value range for Ta/$Co_{20}Fe_{60}B_{20}$/MgO [3,12].

TABLE I. Comparison of MCA (unit: erg/cm^2) between experiments and present calculation.

Expt.		Present calculations	
Structure	MCA	Structure	MCA
Ta/$Co_{20}Fe_{60}B_{20}$/MgO[a]	1.2–1.6	Cu/$Co_{25}Fe_{75}$/MgO	1.453
Au/$Fe_{80}Co_{20}$/MgO[b]	0.65	Au/$Fe_{80}Co_{20}$/MgO	0.676
(V,Cr)/Fe/MgO[c]	1.0	Cu/Fe/MgO	1.472
[Co/Pt(111)]/[Co/Pd(111)][d]	1.15/0.92		

[a]Reference [3].
[b]Reference [23].
[c]Reference [11].
[d]Reference [22].

With the calculated MCA and shape anisotropy, we estimate the critical thickness of the CoFe alloy layer in MgO-MTJs with PMA. For instance, for $Fe_{75}Co_{25}$, the MCA, SAE, and PMA as a function of layer thickness is shown in Fig. 3(a). The MCA is almost constant but with slight oscillations and the absolute value of the SAE is linearly decreasing with increasing layer thickness. The critical thickness with PMA for $Fe_{75}Co_{25}$ is 6 MLs (corresponding to 8.598 Å). Comparing to experiment [3], the critical thickness for $Co_{20}Fe_{60}B_{20}$/MgO/$Co_{20}Fe_{60}B_{20}$-PMTJs is about 1.2–1.5 nm but with the existence of a magnetic dead layer (0.2–0.6 nm). Consequently, our result is within the uncertainties of the experimental values. By using this method, we determine the critical thickness with PMA for different CoFe alloy compositions. The results are shown in Figs. 3(b) and 3(c) for two interesting substrates Cu and MgO, respectively. There is a two dimensional boundary for thickness and composition for realizing PMA and it may be helpful to realize PMA in experiments by using CoFe alloy as electrodes in MgO-MTJs.

The MCA of the whole junction is obtained by summing the band energy difference between perpendicular and in-plane magnetic orientations over all atoms. Although the triple (lms) is not a good quantum number for the full relativistic calculations, the MCA can still be projected into different orbital and spin. In order to understand the origin of large MCA in CoFe/MgO-MTJs, as an illustration, the atom, orbital, and spin resolved MCA contribution for a junction with 3 MLs Fe is shown in Fig. 4. From the top panel in Fig. 4, it becomes clear that the main contributions to the MCA arise from the *d* orbital, whereas *s* and *p* orbitals have relatively smaller contributions. Furthermore, the spin decomposition for the *d* orbital is shown in the bottom panel in Fig. 4. The positive contribution to MCA in the Fe layer is dominated by the spin down channel. This is expected because the spin up channel is almost filled in CoFe alloys.

The atomic resolved band energy difference for the pure materials and three typical CoFe compositions are shown in Fig. 5. The layer-resolved MCA is related to the boundary condition between MgO and substrates. The main contribution to MCA is not only located at FeCo/MgO interface. We found for Fe that the interface Fe monolayer dominates the MCA. For $Fe_{75}Co_{25}$, $Fe_{50}Co_{50}$, positive contributions to the MCA oscillate and extend over the whole magnetic layer, while for Co the largest contribution to MCA is located at the Co/Cu interface.

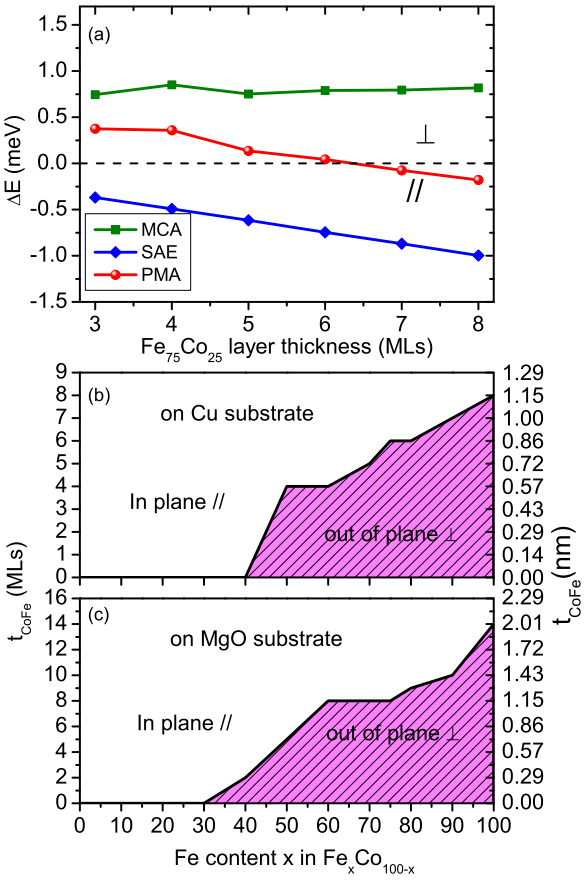

FIG. 3. (Color online) (a) MCA (green square), shape anisotropy energy (blue diamond), and PMA (red circle) per interface in $Cu/Fe_{75}Co_{25}(x$ MLs)/MgO(3 MLs)/$Fe_{75}Co_{25}(x$ MLs)/Cu junction vs the FeCo layer thickness. The CoFe content and layer thickness phase diagram for (b) Cu/Fe_xCo_{100-x} (n MLs)/MgO(3 MLs)/$Fe_xCo_{100-x}(n$ MLs)/Cu, and (c) $MgO/Fe_xCo_{100-x}(n$ MLs)/MgO(3 MLs) with perpendicular easy axis. Left axis is the thickness in units of MLs and the right axis is in units of nm.

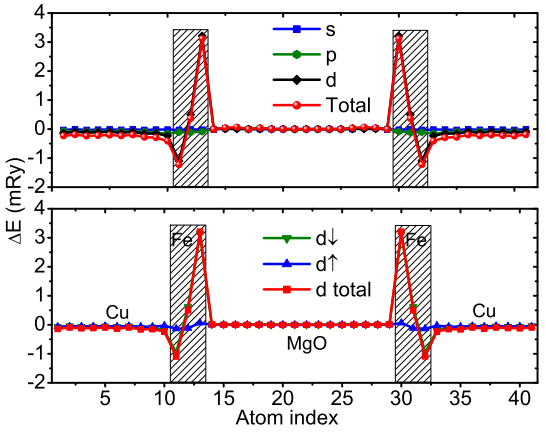

FIG. 4. (Color online) Top: atomic and orbital resolved band energy difference between in-plane and perpendicular magnetic orientations in Cu/Fe(3 MLs)/MgO(3 MLs)/Fe(3 MLs)/Cu junction. Bottom: atomic and spin resolved band energy difference in d orbital.

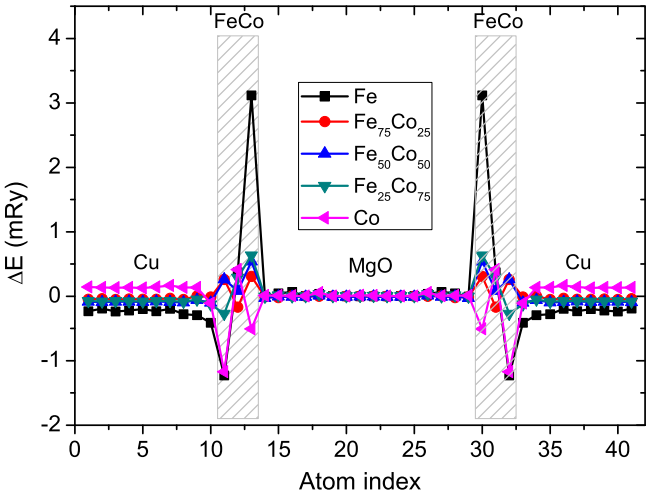

FIG. 5. (Color online) Atomic resolved MCA for $Cu/Fe_xCo_{100-x}(3$ MLs)/MgO(3 MLs)/$Fe_xCo_{100-x}(3$ MLs)/Cu junction with $x = 100$, 75, 50, 25, and 0.

In order to understand the origin and the composition dependence of MCA in CoFe/MgO/CoFe-MTJs, the calculation results will be compared with the theory model of MCA for $3d$ transition metal monolayers. From Bruno's perturbation model for transition metal monolayers [27], the MCA is proportional to the square of the spin-orbit interaction strength ξ (MCA $\sim \xi^2$) and the orbital magnetic moment is proportional to ξ ($\Delta M_L \sim \xi$). This scaling relation can be tested with our first-principles calculations. For the present KKR first-principles method, the spin-orbit interaction strength can be tuned artificially by introducing a scaling factor into the Dirac equation [28]. As an illustration, the calculated MCA and ΔM_L from first principles as a function of spin-orbit interaction strength is shown in Fig. 6. Both MCA as well as ΔM_L agree well with the scaling relation of the model.

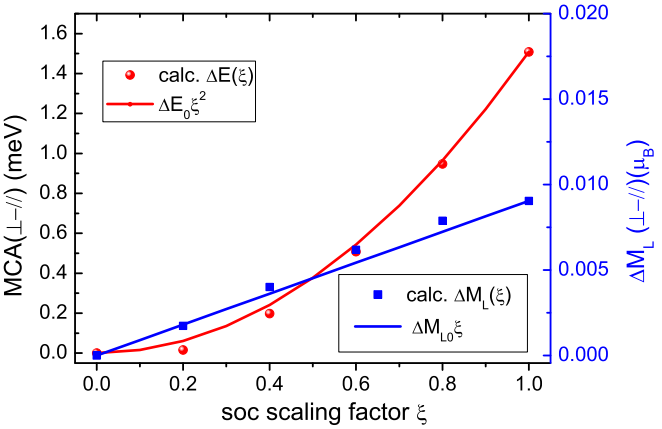

FIG. 6. (Color online) MCA (red) and orbital moment difference $\Delta M_L[M_L(\perp) - M_L(\parallel)]$ on the interface Fe layer (blue) in Cu/Fe(3 MLs)/MgO(3 MLs)/Fe(3 MLs)/Cu junction as a function of soc scaling factor. The circles and squares are calculated data and lines are scaling behavior of Bruno's model. $\xi = 0$ and 1 correspond to the scalar relativistic and full relativistic case, respectively. ΔE_0 and ΔM_{L0} are the calculated values for the full relativistic case.

This suggests that the perturbation model is still applicable for understanding the origin of MCA in CoFe/MgO system. Hereafter, we will discuss the composition dependence of MCA based on perturbation model in detail.

From perturbation theory, it is expected that the MCA in transition metal monolayers is related to excitation between different d orbitals around the Fermi energy [27]. The scalar relativistic density of states (DOS) for d states with different CoFe compositions is calculated and shown in Fig. 7. We can see from the figure that the spin up channel is almost filled and featureless around the Fermi energy, whereas for the spin down channel the density of states changes drastically as a function of CoFe composition. Due to the D_{4h} symmetry of MgO-MTJs, the d_{yz} and d_{zx}, d_{xy} and $d_{x^2-y^2}$ orbitals are degenerated. The shape of the density of states of d_{yz} (or d_{zx}) and $d_{xy}(d_{x^2-y^2})$ are similar especially for CoFe with higher Co content, but $d_{3z^2-r^2}$ is significantly different from them. This is because the $d_{3z^2-r^2}$ orbital in CoFe can be effectively bonded with the interfacial layer but other d orbitals cannot. For example, in Fe/MgO interface the p_z and s orbital in oxygen at the interfacial MgO layer are bonded with the $d_{3z^2-r^2}$ orbital in Fe. This bonding gives rise to the significant difference of density of states between the d orbitals.

Following Bruno's theory [27], by labeling the $3d$ orbital d_{yz}, d_{zx}, d_{xy}, $d_{x^2-dy^2}$, and $d_{3z^2-r^2}$ to 1, 2, 3, 4, and 5 and considering the orbital degeneracy between 1 and 2, 3, and 4, the MCA in CoFe/MgO/CoFe-MTJs can be simplified into

$$K = \tfrac{1}{4}\xi^2\{2I(1,3,1,3) + 3I(1,5,1,5) - \sqrt{3}[I(1,3,1,5) + I(1,5,1,3)]\}.$$

In the above equation, ξ is the spin orbital interaction strength. $I(1,3,1,3)$, $I(1,5,1,5)$, $I(1,3,1,5)$, and $I(1,5,1,3)$ are energy coefficient terms and their definitions are as follows [27]:

$$I(\mu_1,\mu_2,\mu_3,\mu_4) = \mathrm{Re}[G(\mu_1,\mu_2,\mu_3,\mu_4) + G(\mu_2,\mu_1,\mu_4,\mu_3) - G(\mu_1,\mu_2,\mu_4,\mu_3) - G(\mu_2,\mu_1,\mu_3,\mu_4)],$$

$$G(\mu_1,\mu_2,\mu_3,\mu_4) = \sum_{\mathbf{k}} \int_{\varepsilon<\varepsilon_F} d\varepsilon \times \int_{\varepsilon_F<\varepsilon'} d\varepsilon' \frac{m_{\mu_1,\mu_4}(\mathbf{k},\varepsilon) m_{\mu_3,\mu_2}(\mathbf{k},\varepsilon')}{\varepsilon' - \varepsilon}.$$

$m_{\mu_1,\mu_4}(\mathbf{k},\varepsilon)$ and $m_{\mu_3,\mu_2}(\mathbf{k},\varepsilon')$ are the generalized magnetization densities. ε_F is the Fermi energy. These energy coefficient terms $I(1,3,1,3)$, $I(1,5,1,5)$, $I(1,3,1,5)$, and $I(1,5,1,3)$ are relying on the nondegeneracy and difference of DOS between the involved d orbitals around Fermi energy. For instance, the terms $I(1,3,1,3)$ and $I(1,3,1,5)$ and $I(1,5,1,3)$ will turn out to be zero if the orbitals 1 and 3 are degenerated. In addition, because the DOS in spin up channel for five d orbitals are similar and have tiny difference around Fermi energy, these energy terms and MCA are only correlated to the difference of DOS in spin down channel. Indeed, this is consistent with Fig. 4 and hereafter we will only consider the spin down channel.

In CoFe/MgO/CoFe-MTJs because of the lack of symmetry in z direction, the difference between $d_{3z^2-r^2}$ and other d orbitals is significant and eventually leads to the sizable MCA.

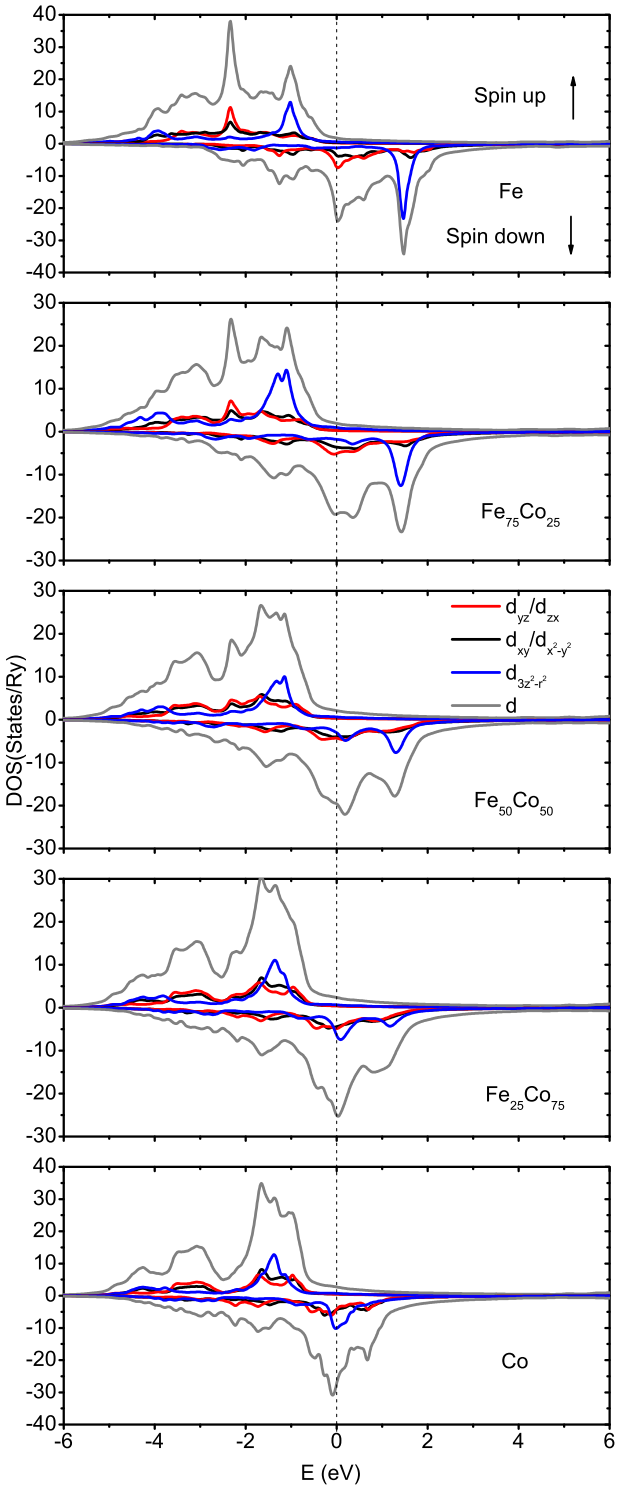

FIG. 7. (Color online) Scalar-relativistic d-orbital density of states (DOS) for two spin channels (positive DOS is for spin up and the sign of DOS for spin down is reversed for plotting) calculated in Fe_xCo_{100-x} atomic layer at which the contribution to MCA is largest in Cu/Fe_xCo_{100-x}(3 MLs)/MgO(3 MLs)/Fe_xCo_{100-x}(3 MLs)/Cu junctions with $x = 100$, 75, 50, 25, and 0. The vertical dash line indicates the position of Fermi energy. Different lines in color correspond to different d orbitals and the gray line is the total DOS for d orbital.

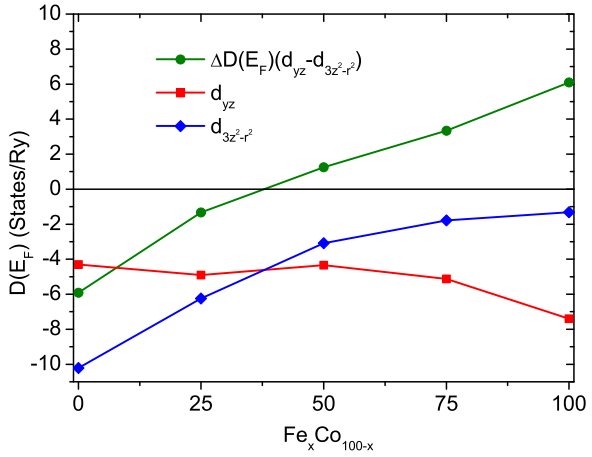

FIG. 8. (Color online) Density of states of spin down channel for d_{yz} and $d_{3z^2-r^2}$ and their difference at Fermi energy for the layer shown in Fig. 7.

As we mentioned previously, the shape of DOS of orbitals 1 and 3 is similar. Thus the difference of DOS between d_{yz} (or d_{zx}) and $d_{3z^2-r^2}$ will be dominating and the leading contribution to the MCA. We can qualitatively relate the MCA in CoFe/MgO/CoFe-MTJs to the difference of density of states between d_{yz} (or d_{zx}) and $d_{3z^2-r^2}$ orbitals at the Fermi energy. The DOS of d_{yz} (or d_{zx}), $d_{3z^2-r^2}$ and their difference is plotted in Fig. 8. One can see that the DOS difference decreases with increasing Co content. Further, at a certain composition there is also a sign change similar to the MCA. This composition is close to the composition where we have a transition for the MCA shown in Fig. 2.

In summary, we investigate the origin and alloy composition dependence of PMA in CoFe/MgO/CoFe-MTJs. We show that the MCA decreases with increasing Co content. The critical thickness with PMA for various CoFe concentration is also determined by taking the shape anisotropy into account. We find that the d orbital splitting, especially between the d_{yz} and $d_{3z^2-r^2}$ orbitals, plays a crucial role for high MCA in MgO-MTJs. However, the enhancement of spin orbit strength, for example with noble metal Au substrate, is less important. The CoFe composition dependence of the MCA can be well explained by perturbation theory and the evaluation of the density of states around the Fermi energy. Besides the enhancement of the spin orbit coupling the increase of the d orbital splitting may be more important for achieving high MCA in MgO-MTJs.

We thank M. Münzenberg for useful discussions and acknowledge support from Deutsche Forschungsgemeinschaft (SPP 1538 and Grant No. HE 5922/1-1).

[1] S. Mangin, D. Ravelosona, J. A. Katine, M. J. Carey, B. D. Terris, and E. E. Fullerton, Nat. Mater. **5**, 210 (2006).
[2] T. Kishi, H. Yoda, T. Kai, T. Nagase, E. Kitagawa, M. Yoshikawa, K. Nishiyama, T. Daibou, M. Nagamine, M. Amano, S. Takahashi, M. Nakayama, N. Shimomura, H. Aikawa, S. Ikegawa, S. Yuasa, K. Yakushiji, H. Kubota, A. Fukushima, M. Oogane, T. Miyazaki, and K. Ando, in *IEEE International Electron Devices Meeting, San Francisco, CA* (IEEE, Piscataway, NJ, 2008), pp. 1-4.
[3] S. Ikeda, K. Miura, H. Yamamoto, K. Mizunuma, H. D. Gan, M. Endo, S. Kanai, J. Hayakawa, F. Matsukura, and H. Ohno, Nat. Mater. **9**, 721 (2010).
[4] S. Yakata, H. Kubota, Y. Suzuki, K. Yakushiji, A. Fukushima, S. Yuasa, and K. Ando, J. Appl. Phys. **105**, 07D131 (2009)
[5] M. Yoshikawa, E. Kitagawa, T. Nagase, T. Daibou, M. Nagamine, K. Nishiyama, T. Kishi, and H. Yoda, IEEE Trans. Magn. **44**, 2573 (2008).
[6] G. Kim, Y. Sakuraba, M. Oogane, Y. Ando, and T. Miyazaki, Appl. Phys. Lett. **92**, 172502 (2008).
[7] K. Mizunuma, S. Ikeda, J. H. Park, H. Yamamoto, H. Gan, K. Miura, H. Hasegawa, J. Hayakawa, F. Matsukura, and H. Ohno, Appl. Phys. Lett. **95**, 232516 (2009).
[8] S. Ikeda, J. Hayakawa, Y. Ashizawa, Y. M. Lee, K. Miura, H. Hasegawa, M. Tsunoda, F. Matsukura, and H. Ohno, Appl. Phys. Lett. **93**, 082508 (2008).
[9] W. X. Wang, Y. Yang, H. Naganuma, Y. Ando, R. C. Yu, and X. F. Han, Appl. Phys. Lett. **99**, 012502 (2011).
[10] C. W. Cheng, W. Feng, G. Chern, C. M. Lee, and T. Wu, J. Appl. Phys. **110**, 033916 (2011).
[11] C. H. Lambert, A. Rajanikanth, T. Hauet, S. Mangin, E. E. Fullerton, and S. Andrieu, Appl. Phys. Lett. **102**, 122410 (2013).
[12] Q. L. Ma, S. Iihama, T. Kubota, X. M. Zhang, S. Mizukami, Y. Ando, and T. Miyazaki, Appl. Phys. Lett. **101**, 122414 (2012).
[13] G. H. O. Daalderop, P. J. Kelly, and M. F. H. Schuurmans, Phys. Rev. B **41**, 11919 (1990).
[14] L. Szunyogh, B. Ujfalussy, and P. Weinberger, Phys. Rev. B **51**, 9552 (1995).
[15] R. H. Victora and J. M. MacLaren, Phys. Rev. B **47**, 11583 (1993).
[16] H. X. Yang, M. Chshiev, B. Dieny, J. H. Lee, A. Manchon, and K. H. Shin, Phys. Rev. B **84**, 054401 (2011).
[17] X. G. Zhang and W. H. Butler, Phys. Rev. B **70**, 172407 (2004).
[18] C. Franz, M. Czerner, and C. Heiliger, Phys. Rev. B **88**, 094421 (2013).
[19] Y. M. Lee, J. Hayakawa, S. Ikeda, F. Matsukura, and H. Ohno, Appl. Phys. Lett. **90**, 212507 (2007).
[20] F. Bonell, T. Hauet, S. Andrieu, F. Bertran, P. Le Fevre, L. Calmels, A. Tejeda, F. Montaigne, B. Warot-Fonrose, B. Belhadji, A. Nicolaou, and A. Taleb-Ibrahimi, Phys. Rev. Lett. **108**, 176602 (2012).
[21] T. Devolder, P. H. Ducrot, J. P. Adam, I. Barisic, N. Vernier, J.-V. Kim, B. Ockert, and D. Ravelosona, Appl. Phys. Lett. **102**, 022407 (2013).

[22] M. Johnson, P. J. H. Bloemen, F. J. Broeder, and J. J. Vries, Rep. Prog. Phys. **59**, 1409 (1996).

[23] Y. Shiota, T. Maruyama, T. Nozaki, T. Shinjo, M. Shiraishi, and Y. Suzuki, Appl. Phys. Express **2**, 063001 (2009).

[24] J. Zabloudil, R. Hammerling, L. Szunyogh, and P. Weinberger, *Electron Scattering in Solid Matter: A Theoretical and Computational Treatise*, Springer Series in Solid-State Sciences, Vol. 147 (Springer, Berlin, 2005).

[25] C. Etz, B. Lazarovits, J. Zabloudil, R. Hammerling, B. Ujfalussy, L. Szunyogh, G. M. Stocks, and P. Weinberger, Phys. Rev. B **75**, 245432 (2007).

[26] S. Bornemann, J. Minr, J. Braun, D. Kdderitzsch, and H. Ebert, Solid State Commun. **152**, 85 (2012).

[27] P. Bruno, Phys. Rev. B **39**, 865 (1989).

[28] H. Ebert, H. Freyer, A. Vernes, and G.-Y. Guo, Phys. Rev. B **53**, 7721 (1996).